

Supporting Information

In order to validate our experimental results, three-dimensional finite-volume method (FVM) simulations were performed only for the Newtonian case. The aim of this numerical work was to quantify accurately the errors in our experimental measurements with respect to the real untethered case, basically due to the presence of the support and the depth of measurement of the μ PIV technique. The SP model and the Newtonian blood analogue fluid were used for both the experiments and the CFD analysis. On one hand, numerical predictions obtained for the model without cylindrical support was considered as the reference values to evaluate these errors. On the other hand, we also carried out a second set of simulations, with the same physical parameters than those used in the untethered cases, but including the cylindrical support.

Steady state simulations were developed by means of the open source CFD package OpenFOAM[®]. The common solver *simpleFoam* and a laminar transport model were used, together with second order bounded schemes for the convective terms of the Navier-Stokes equations¹. The governing equations used in flow dynamics are expressed as:

$$\nabla \cdot \vec{u} = 0 \quad (1)$$

$$\rho \vec{u} \cdot \nabla \vec{u} = -\nabla p + \eta \nabla^2 \vec{u} \quad (2)$$

where ρ is the fluid density, \vec{v} is the velocity field, p is the pressure and η is the constant viscosity.

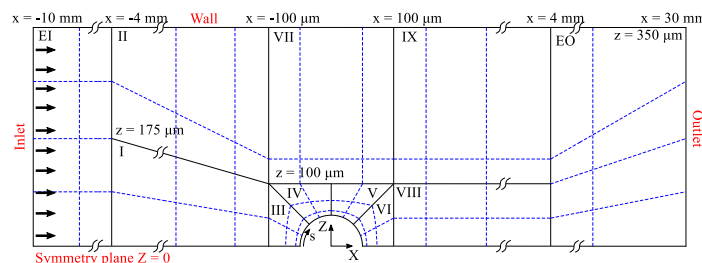


Fig. S.1 Block scheme and base hexahedral mesh (dashed lines) at the mid-plane $Y = 0$.

The fluid-domain was represented by a straight microchannel with $700 \times 700 \mu\text{m}$ square cross-section. The SP model of $50 \mu\text{m}$ radius was placed at the center of the square cross-section and separated far away enough from the inlet and outlet sections to avoid entry and exit effects at the measurement zone. Boundary conditions for velocity field included: an uniform profile at the inlet section; no-slip condition at the walls, model and support surfaces; symmetry at the two longitudinal planes $Y = 0$ and $Z = 0$ for the untethered simulations (a quarter of channel was simulated) and only at the longitudinal plane $Z = 0$ for the with-support simulations (half of channel was simulated); and a Neumann condition at the outlet section, setting the velocity derivative to zero in the flow direction. Boundary conditions for the momentum equation also include the value of static pressure sets to zero at the outlet section.

The three-dimensional fluid-domain was divided into blocks in order to carry out a structured hexahedral mesh. A representation of these blocks at the channel mid-plane and the base mesh are depicted in Fig. S.1. A mesh analysis with five different size meshes and Newtonian fluid behavior was developed for the two-dimensional (2D) case, represented by the microchannel mid-plane $Y = 0$. The mesh refinement level was increased progressively in the near field of the SP model. To provide a quantitative comparison of the mesh refinement effects, we used two kind of parameters: an integral parameter as the deviation of the pressure component of the drag force on the model (ΔF_{Xpress})²; and two parameters (PNE and APNE) to quantify velocity errors along the center line of the rear wake ($z = 0$) and the line perpendicular to the stream direction at the center of the model ($x = 0$), as in Favero et al³. The PNE and the APNE are the percentage normalized error and the average percentage normalized error, respectively. These two parameters were used to provide a quantitative comparison of the mesh refinement effects. These parameters are defined in the following way:

$$\text{PNE} = \max \left(\frac{|U_j - U_j^{ref}|}{\max(|U^{ref}|)} \right) \times 100 \quad (3)$$

$$\text{APNE} = \frac{\sum_{j=1}^N |U_j - U_j^{ref}| / \max(|U^{ref}|)}{N} \times 100 \quad (4)$$

where U_j is the value of the fluid velocity X -component U at a point j of the mesh along the considered profile, U_j^{ref} is the interpolated value of U in the same point for the reference case, and N is the number of discretization points on the considered profile. The superscript *ref* always indicates the values obtained for the mesh M120, which was selected as reference case. Dimensional features and sizes of the five meshes are shown in Table S.1, together with results for the mesh convergence parameters. The mesh M120 was taken as reference to evaluate the refinement effects. Results showed that the obtained PNE value for the velocity profile at the line $x = 0$ was only acceptable for the meshes M80 and M100. Taking into account these results and the projected size of the three-dimensional resulting meshes, it is obvious that the M100 mesh refinement level ensures a high accuracy on the velocity field prediction with an acceptable computational cost. Therefore, the 3D mesh for the SP model was built dividing the fluid-domain with the block scheme that shown in Fig. S.1 and with the M100 refinement parameters also extended on the third dimension.

Five cases were simulated for the untethered and with-support models, corresponding to $Re_c = 0.1, 1.02, 10.2$ and 51.1 and results from both sets of simulations were processed to obtain a correction factor K_p . This factor K_p is defined point-to-point for each measurement plane Y as a percentage quantity of U_m which is added to the velocity value measured on that point:

$$u_p^* = u_p + K_p \cdot U_m \quad (5)$$

where u_p^* , u_p and K_p are the corrected experimental velocity, the μ PIV measured velocity and the obtained corrector factor at a point

Table S.1 Dimensional features of the five 2D meshes and convergence results.

	M40	M60	M80	M100	M120
N_s	40	60	80	100	120
N_r ($x = 0$)	25	35	45	55	65
$\{\Delta s/R_1\}_{min}$	0.078	0.052	0.039	0.031	0.026
$\{\Delta r/R_1\}_{min}$	0.016	0.012	0.010	0.008	0.006
Cells	66600	221850	520800	1013750	1747800
$\Delta F_{X_{press}}$ [%]	-0.77	-0.28	-0.12	-0.03	-
PNE at $z = 0$	0.83	0.70	0.14	0.05	-
APNE at $z = 0$	0.28	0.13	0.042	0.016	-
PNE at $z = 0$	6.84	2.27	0.79	0.29	-
APNE at $z = 0$	0.88	0.33	0.15	0.07	-

p of a plane Y , respectively. Due to the geometry of the studied flow, the streamwise velocity field give much more representative information about the flow features than the cross-stream direction velocity field, and this is why we focused only on the streamwise velocity correction. However a similar process could be applied to the cross-stream direction velocity at the plane Y .

The factor K_p considers two error sources in each point p : the error introduced by the presence of the cylindrical support (k_{1p}) and the error due to the optical depth of measurement (k_{2p}), then $K_p = k_{1p} + k_{2p}$. Firstly, the presence of the cylindrical support increases the blockage ratio at the microchannel cross-section and consequently leads to higher velocities of the fluid at the contraction created by the model. For a given Y -plane this error is quantify point-to-point by the factor k_{1p} , defined as the following way:

$$k_{1p} = \frac{\{u'_p\}_{unt} - \{u'_p\}_{wsup}}{U'_m} \quad (6)$$

$\{u'_p\}_{unt}$, $\{u'_p\}_{wsup}$ being the numerical predicted velocity at the point p for the untethered and with-support simulations, respectively; and U'_m the numerical mean velocity in the channel. Maximum values for the factor k_{1p} are reached at the microchannel centerplane $Y = 0$ for the lowest Reynolds number case and its maximum value was ~ 0.1 .

Secondly, in a μ PIV setup the entire depth of the channel is illuminated by the laser light and hence the thickness of the measurement plane is defined by the depth of field of the microscope objective. This thickness is usually expressed in terms of depth of correlation (DOC), which is defined as twice the distance from the focal plane to the nearest plane in which a particle becomes sufficiently defocused to not contribute to the cross-correlation analysis⁴. The depth of correlation and the interrogation area chosen for the cross-correlation analysis define the interrogation volume. Therefore the velocity value measured at a certain position is given by a weighted average of the particles contained in that interrogation volume⁵. For the case of a microchannel with a circular cylinder placed in the square cross-section centerline (typically considered as the two-dimensional case of the flow around a sphere), the velocity at any point of a plane contained in the interrogation volume remains almost unchanged with respect to that in the center plane of the interrogation volume. However, our three-dimensional microbot model causes secondary flows perpendicular to the focal plane in the near field of the sphere. This may lead to velocity fields in planes above and below the focal plane

quite different to the velocity field in the focal plane. Therefore, a deviation on the obtained velocities exists since the measured value at a point is a weighted average of the velocities at the same point along the Y -direction of the interrogation volume. This error was quantify point-to-point for each measurement plane Y by means of the factor k_{2p} , defined as:

$$k_{2p} = \frac{\{u'_p\}_0 - \overline{u'_p}}{U'_m} \quad (7)$$

where $\{u'_p\}_0$ is the numerical velocity predicted at the point p at the focal plane and $\overline{u'_p}$ is the weighted average of the velocity along the Y -direction of the interrogation volume at the same point p evaluated from the numerical results. This correction factor k_{2p} was estimated from the with-support simulations results, applying the formulation developed by Rossi et al.⁶ to calculate the effective depths of correlation (DOC) and the corresponding weighting functions $W(y)$ for the μ PIV setup used (equations 11-16 in Rossi et al.⁶). Results for effective depths of correlation of the lenses used in this work are shown in Table S.2.

Table S.2 Characteristic parameters for the objectives used in the μ PIV measurements and their effective Depths of Correlation.

Magn. (M)	NA	c_d ⁶	DOC [μ m]
10x	0.30	0.80	48.1
20x	0.40	0.75	30.9

To calculate $\overline{u'_p}$, a discrete sample of the velocity at the same point p in N Y -planes separated $\Delta y = 5 \mu$ m each other within the interval $-DOC/2 \leq y_n \leq +DOC/2$ was taken and averaged using the weighting function. Therefore, $\overline{u'_p}$ can be expressed in the following terms:

$$\overline{u'_p} = \frac{\sum_{n=1}^N \{u'_p\}_n \cdot W(y_n)}{\sum_{n=1}^N W(y_n)} \quad (8)$$

where $\{u'_p\}_n$ and $W(y_n)$ are the velocity at the point p and the weighting function value, respectively, at the Y -plane n . The maximum values for the correction factor k_2 are given at the plane $Y = +50 \mu$ m due to the presence of the model above the focal plane and a free-obstacles flow below it. The maximum value for k_2 was ~ 0.06 , just at the point where the 3D model is tangential to the focal plane.

The lens $M = 20x$ was used to measure velocity at several planes from $Y = 0$ to $Y = +70 \mu$ m for $Re_c = 1.02$ case. An interrogation area of 32×64 pixels and 50% overlap was chosen for the cross-correlation analysis, giving velocity values each $5.92 \times 11.84 \mu$ m. Fig. S.2[a] depicts the raw and corrected streamwise velocity u^* profiles at the centerline of each Y -plane, together with the numerical results for the untethered SP model. Corrected experimental velocity fields and numerical prediction for the spherical microbot model are roughly in good agreement. However, the most unfavorable measurement plane correspond to $Y = +50 \mu$ m, where any slight deviation on the focal plane Y -positioning may cause such a big difference between the experimental value and the numerical velocity prediction, especially at the point $x = z = 0$ (SP model tangential to the focal plane). Furthermore, the lens $M = 10x$ was also used to obtain velocity measurements in the chan-

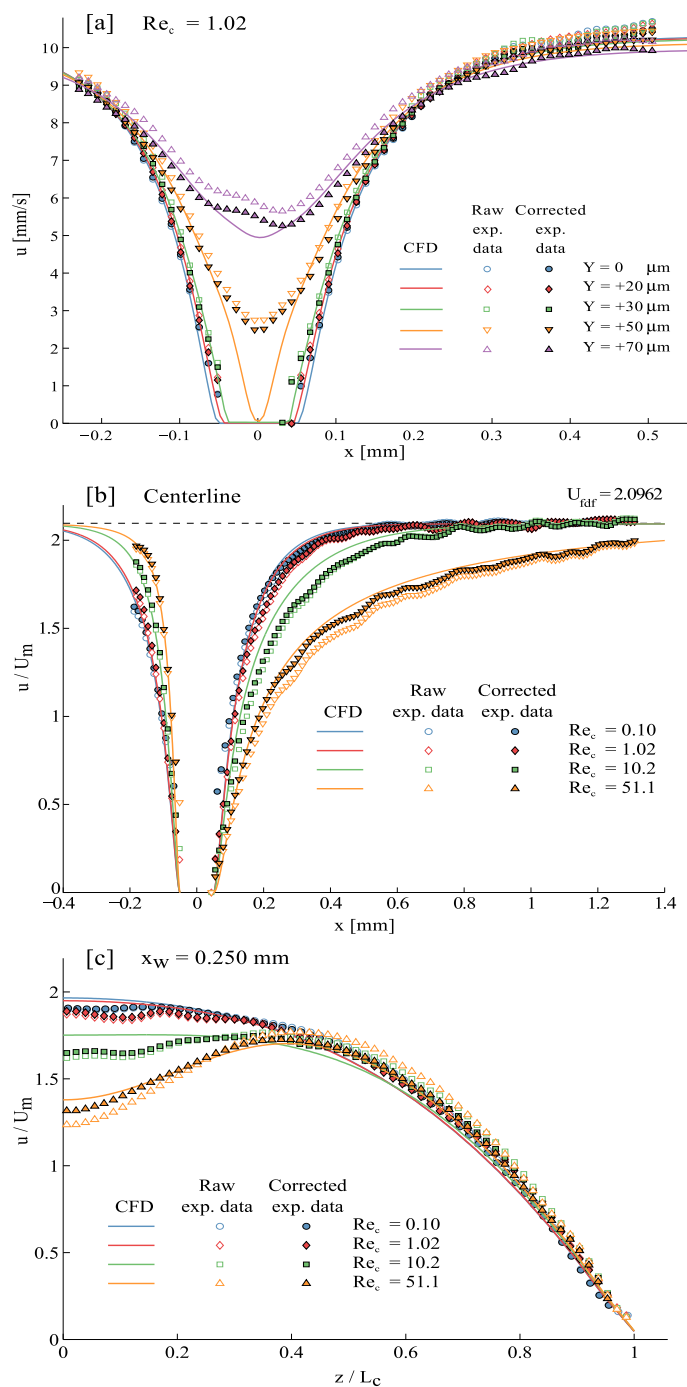


Fig. S.2 Raw and corrected experimental streamwise velocity u^* profiles with Newtonian blood analogue fluid and numerical prediction for the untethered SP model: [a] Streamwise velocity at the centerline of each Y -plane for $Re_c = 1.02$; [b] Normalized streamwise velocity at the mid-plane centerline and [c] at the mid-plane cross-stream direction line at $x_w = 250 \mu\text{m}$, for different Re_c .

nel mid-plane ($Y = 0$) for Reynolds numbers in the channel 0.1, 1.02, 10.2 and 51.1. For this lens, an interrogation area of 16×32 pixels and 50% overlap was chosen for the cross-correlation analysis, giving the same grid for the velocity field. Fig. S.2[b] and [c] depicts the normalized velocity profiles at the microchannel centerline and the cross-stream direction line at $x_w = 250 \mu\text{m}$, being x_w the distance downstream of the rear stagnation point on the model surface. Again numerical and experimental results are in good agreement. Comparison between numerical and experimental data enables to ensure that the velocity values measured by μPIV are representative of the real untethered model dynamics and even to quantify the experimental errors derived from our set-up.

References

- 1 H. K. Versteeg, W. Malalasekera, An Introduction to Computational Fluid Dynamics, Longman Scientific & Technical, Essex, UK, 1995.
- 2 M. A. Alves, F. T. Pinho, P. J. Oliveira, Study of steady pipe and channel flows of a single-mode phan-thien-Åstanner fluid, J. Non-Newtonian Fluid Mechanics 101 (2001) 55–76. Doi:10.1016/S0377-0257(01)00159-8.
- 3 J. L. Favero, A. R. Secchi, N. S. M. Cardozo, H. Jasak, Viscoelastic flow analysis using the software openfoam and differential constitutive equations, J. Non-Newtonian Fluid Mechanics 165 (2010) 1625–1636. Doi:10.1016/j.jnnfm.2010.08.010.
- 4 C. D. Meinhart, S. T. Wereley, M. H. B. Gray, Volume illumination for two-dimensional particle image velocimetry, Measurement Science and Technology 11 (2000) 809. Doi:10.1088/0957-0233/11/6/326.
- 5 M. G. Olsen, R. J. Adrian, Out-of-focus effects on particle image visibility and correlation in microscopic particle image velocimetry, Experiments in Fluids 29 (2000) S166–S174. Doi:10.1007/s003480070018.
- 6 M. Rossi, R. Segura, C. Cierpka, C. J. Kahler, On the effect of particle image intensity and image preprocessing on the depth of correlation in micro-PIV, Experiments in Fluids 52 (2012) 1063–1075. Doi:10.1007/s00348-011-1194-z.